Enhancement of water remediation by innovative photocatalytic luminous textiles reactor: Performance, kinetic modeling, and mechanistic insights

Sarra Karoui, Aymen Amine Assadi, Achraf Ghorbal, Lotfi Khezami, Achraf Assadi, Sivachandiran Loganathan, Abdeltif Amrane

Enhancement of Water Remediation by Innovative Photocatalytic Luminous Textiles Reactor: Performance, Kinetic Modeling, and Mechanistic Insights

Sarra Karoui [a,b], Aymen Amin Assadi [c,d], Achraf Ghorbal [a], Lotfi Khezami[e], Achraf Assadi[a,f], Sivachandiran loganathan[g], Abdeltif Amrane [d]

[a]Research Unit, 2MPE, Advanced Materials, Applied Mechanics, Innovative Processes and Environment, UR22ES04, Higher Institute of Applied Sciences and Technology of Gabes, University of Gabes, Tunisia

[b]Laboratoire de Réactivité de Surface (LRS), UMR 7197 CNRS - Sorbonne Université, Campus Pierre et Marie Curie, 4 place Jussieu, F-75005, Paris, France

[c]College of Engineering, Imam Mohammad Ibn Saud Islamic University, IMSIU, Riyadh 11432, Saudi Arabia

[d]Univ Rennes, Ecole Nationale Supérieure de Chimie de Rennes, CNRS, ISCR, UMR 6226, F-35000 Rennes, France

[e]Chemistry Department, College of Science, Imam Mohammad Ibn Saud Islamic University (IMSIU), Riyadh 11432, Saudi Arabia

[f]Center for Research on Microelectronics and Nanotechnology, CRMN Sousse Techno Park, Sahloul BP 334, Sousse 4054, Tunisia

[g]Plasma Research Laboratory, Department of Chemical and Biomolecular Engineering, Center for Air and Aquatic Resources Engineering & Science, Clarkson University, Potsdam, NY 13699, USA

* Corresponding author. E-mail address: aymen.assadi@ensc-rennes.fr (A.A. Assadi)

Abstract

To address wastewater treatment, a photocatalytic process using luminous-textile has been proposed due to its high efficiency and non-toxicity. In the present work, the photodegradation of Ciprofloxacin (CIP) in the liquid phase was studied in a compact reactor with a luminous-textile catalyst in three different configurations: (i) “mono-face” (MF), (ii) “double-face” (DF) and (iii) “double-face without TiO_2” (DF-without TiO_2). The DF configuration exhibited the highest efficiency for CIP removal (99.7%) and mineralization (40.3%), followed by MF and DF-without TiO_2. The DF luminous textiles, before and after CIP degradation, were characterized using scanning electron microscope and Fourier-transform infrared spectroscopy. The effect of operating parameters, such as CIP initial concentration (2 - 10 mg/L) and UV light intensity (0.08, 0.15 and 0.26 mW/cm^2) on luminous-textile performance in terms

of CIP degradation efficiency and mineralization yield was investigated. Good photocatalytic activity was found with 2 mg/L CIP initial concentration and 0.15 mW/cm^2 UV light intensity. Moreover, the mineralization percentage reached 54.7% and 61.2% with the addition of 150 mg/L of H_2O_2 and 202 mg/L of PS, respectively. Additionally, the impact of radical scavengers was studied, proving that $HO_2^{\bullet}$, $O_2^{-\bullet}$, and especially radicals were the basic active species involved in CIP degradation mechanism.

Furthermore, the degradation efficiency decreased from 99.7% in ultra-pure water to 63.6% in tap water (TW) and 46.1% in synthetic water (SW), demonstrating the negative effects of nitrate, chloride, sulfate and bicarbonate ions on CIP degradation and mineralization efficiencies in TW and SW. In summary, the present study unraveled the mechanistic aspects of the excellent photocatalytic ability of the luminous-textile for the CIP mineralization.

Keywords: Luminous textiles; Compactness reactor; Photocatalysis, wastewater; Kinetic enhancement; reactive species

1. Introduction

Industrial wastewater containing organic contaminants poses a significant threat to human health and environment [1]. These hazardous organic compounds are chemically stable and non-biodegradable [2], making their removal from aquatic environments challenging using non-destructive techniques, such as flocculation [3], adsorption [4], coagulation and/or filtration [5,6]. Chemical and biological processes like chemical oxidation, plasma, disinfection/ozonation and chlorination, although effective for water treatment, can generate toxic by-products [7,8]. Therefore, there is

a need for innovative treatment methods capable of completely removing persistent contaminants.

Heterogeneous photocatalysis, an efficient and eco-friendly advanced oxidation process (AOP), offers distinct advantages over other treatment techniques. It can effectively degrade target molecules, leading to high mineralization [9–11]. This process can efficiently mineralize numerous drugs, transforming them into comparatively non-toxic final products such as water (H_2O) and carbon dioxide (CO_2) [12]. The TiO_2 is a widely used photocatalytic semiconductor, known for its high surface area, affordability , low toxicity, photochemical stability, and commercial availability [12].

However, the reactor used in the photocatalytic process typically relies on external light, which can be extremely energy-intensive (20–150 W) for a relatively low durability, usually around 1000 h [13]. Consequently, optimizing the contact between the catalyst, the light, and the contaminant has become a primary challenge to overcome poor light penetration. To address this issue, researchers have proposed to use of immobilized photocatalysts and TiO_2 coated optical-fibers as a promising technique for the environmental depollution [14].

Recently, luminous textiles have been explored for photocatalytic water treatment, wherein optical-fibers are connected to an ultraviolet light-emitting-diode (UV-LED) source. Luminous photocatalytic textiles offer several advantages; (i) They enhance the interactions between the solution and the support, (ii) They consume less energy through optimized LED usage , and (iii) They optimize the contact between the photocatalyst support and the transmitted light [14]. The performance of luminous textiles has been evaluated for the degradation of various air pollutants, including formaldehyde [13], toluene and acetic acid [15], Butane-2,3-dione, and Heptan-2-one

[16], as well as chloroform and glutaraldehyde [17]. However, only a limited number of research works have reported the use of luminous textiles for removing antibiotics from wastewater [18].

In the present study, the antibiotic Ciprofloxacin (CIP) was chosen as the model pollutant molecule. This synthetic antibiotic is frequently detected in water sources at concentrations ranging from 1 µg/L to 31 mg/L [19]. The presence of CIP in the aquatic environment contributes to the development of antibiotic-resistant bacteria [20], posing a threat to both human health and the environment. Various advanced oxidation processes have been employed to remove CIP antibiotic, including the AOP method with Ferrate (VI) from Extreme Base Electrosynthesis [21], Co–Mn oxide supported by carbon fiber frameworks [22] electro-coagulation using iron electrodes, and electro-peroxone application [23,24]. The primary objective of this paper is to investigate the CIP degradation efficiency of the compact photocatalytic batch reactor. To the best of our knowledge, the photodegradation of CIP using luminous photocatalytic textiles has not been previously reported. A comparative study between three different configurations of luminous textile reactors is conducted. The influence of CIP initial concentration and UV light intensity on removal and mineralization efficiency is examined using the most efficient design. Furthermore, an intriguing challenge is addressed in this study: the impact of the addition of oxidants, specifically hydrogen peroxide and persulfate, on CIP mineralization is investigated.

This study represents the first investigation in which hydrogen peroxide and persulfate oxidants are added to a compact reactor with a luminous textile catalyst to enhance CIP degradation. The types of radicals and their role in CIP mineralization are also explored using external radical scavengers. Finally, the photocatalytic performance of luminous textiles in various water matrices is assessed to understand

the effects of other ions present in the water. To our knowledge, no previous work has focused on the treatment of various water matrices using a compact reactor with a luminous textile catalyst for CIP removal.

2. Materials and methods

2.1 Chemicals

Ciprofloxacin (CIP, $C_{17}H_{18}FN_3O_3$, purity = 98%) was purchased from Merck. Isopropanol (IPA, C_3H_8O, purity ≥ 99.9%), 1,4-Benzoquinone (BQ, $C_6H_4O_2$) and Tert-butanol (t-BuOH, $C_4H_{10}O$) were purchased from Merck. All chemicals were used without any purification. Ultra-pure-water supplied from a Millipore-Milli-Q system was used to prepare all solutions. Hydrogen peroxide (H_2O_2) and potassium persulfate (PS, $K_2S_2O_8$, purity ≥ 99.9%) were purchased from sigma Aldrich.

2.2 Catalysts description

The catalysts were purchased from the Brochier Technologies Company (UVtex®). The luminous textile consisted of a combination of optical-fibers, made of polymethyl methacrylate resin (PMMA CK-20 Eska™ fibres), and textiles-fibers made of polyester (Trévira CS™ fibres). The detailed procedure for preparing the catalyst was previously documented by Almansba et al. [18]. The optical fibers had an average diameter of 480 µm and were coated with a 10 µm-thick layer of fluorinated polymer [25]. The textile fibers were composed of TiO_2 (mixture of zeolite, silica and TiO_2 Millennium PC500) deposited on non-woven cellulose-fibers [26] , with a deposit thickness of 250 µm. The catalyst's active surface area measured 3 10^{-2} m^2 and it was purchased from the Ahlstrom Company (Alhstrom 1048). Jacquard loom was employed to interlace the optical and textile-fibers together. To elaborate, the optical fibers were arranged vertically, whilethe textile fibers were positioned horizontally. All

the optical fibers were converged on one side, which was then exposed to UV light. They were connected to a cylindrical aluminum connector securely fastened with silicone (GP-LC7021-0A).

Three different luminous textiles were subjected to testing for the photocatalytic degradation of CIP. These included: (i) “mono-face” (MF), (ii) the “double-face” (DF), and (iii) the “double-face without TiO_2” (DF-without TiO_2). Both the MF and DF configurations were coated with a similar quantity of TiO_2. However, these two configurations had different distributions of optical fibers. In the case of the DF, optical fibers were distributed on two sides, while the MF had them on only one side. . Approximately 0.36 g of TiO_2 was deposited on both the DF and MF supports. Notably, the DF-without TiO_2 reactor did not contain any TiO_2 particles on its surface. . All of the luminous textiles utilized in the study had the same active surface area, measuring 30 x 10 cm^2 in size.

2.3 Photocatalytic experiments

The photocatalytic degradation of the antibiotic CIP in solution was conducted within a 2 L glass batch reactor. In each experiment, 2 L of the CIP solution was introduced into the reactor, and the luminous textile catalyst was submerged in the center of the reaction solution. An LED (Light Emitting Diode) emitting light at a peak wavelength of 365 nm served as the light source, offering energy-efficient operation. **Figure 1** illustrates the schematic representation of photocatalytic reactor employed for CIP treatment.

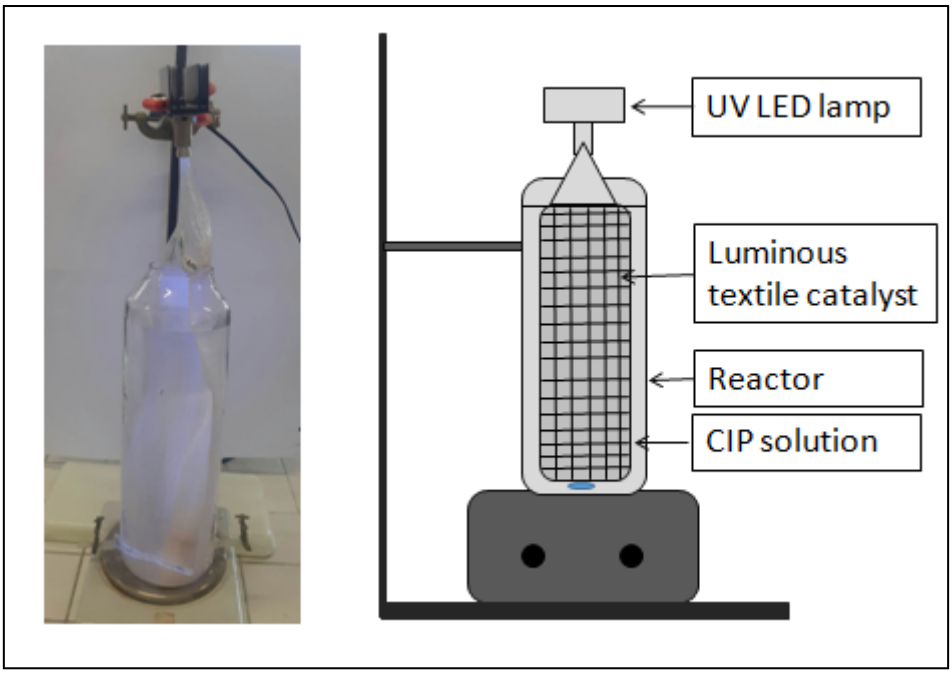

Fig.1 - Schematic representation of photocatalytic reactor employed for CIP treatment.

As described in our previous paper, which was reported by [27], the synthetic wastewater (SW) was prepared in tap water (TW) by adding the following components:1 g/L of NaCl, 230 mg/L of Na_2HPO_4, 50 mg/L of citric acid, 30 mg/L ascorbic acid and 100 mg/L of saccharose. This SW was formulated to replicate the composition of hospital wastewater.

2.4 Characterization methods

The chemical compositions of luminous textiles before and after CIP photodegradation were assessed using Fourier-Transform-Infrared Spectroscopy (FTIR, PerkinElmer, USA) and Scanning-Electron-Microscopy (SEM, IT 300). The FTIR spectrometer was equipped with an Attenuated-Total-Reflectance (ATR) crystal accessory and Deuterated-Glycine-Sulfate (DTGS) detector, and four scans were conducted with a resolution of 2 $cm^{-1.}$

2.5 Analytical method

The CIP concentration was monitored using a UV–Vis spectrophotometry (Cary 50 probe, Varian) at a fixed wavelength of 273 nm. The CIP degradation efficiency was calculated using Eq. 1:

$$\text{CIP degradation efficiency } (\%) = \frac{C_0 - C_t}{C_0} * 100 \qquad \text{Eq. 1}$$

Where C_0 and C_t are the CIP concentration of initial and at time t (mg/L), respectively.

The mineralization of CIP, observed at various photocatalytic treatment times, was monitored using a total organic carbon (TOC) analyzer (Shimadzu A-200, Tokyo, Japan). The mineralization efficiency was calculated employing Eq. 2:

$$\text{Mineralization efficiency } (\%) = \frac{\text{TOC}_0 - \text{TOC}_t}{\text{TOC}_0} * 100 \qquad \text{Eq. 2}$$

Where, TOC_0 and TOC_t are the organic carbon concentration of initial and at time t, respectively (mg/L).

3. Results and discussions

3.1 Characterization of the luminous textiles

Surface analysis via SEM images was utilized to obtain insights into the morphology and structure of the catalyst, as depicted in **Fig. 2.** The SEM image clearly illustrates an entanglement between the optical and textile fibers, creating attachment points. Moreover, it is evident that TiO_2 has been uniformly deposited on the fibers. A similar result was also reported by Indermühle et al., [14]**.**

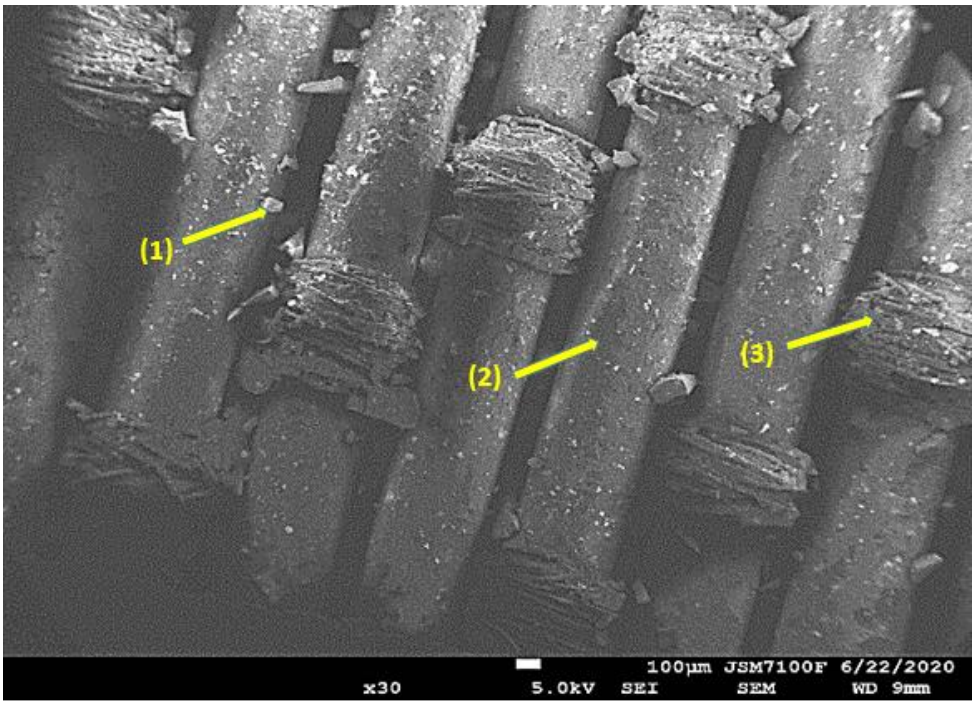

Fig. 2 - SEM image of TiO_2 deposited luminous textile. (1) TiO_2 particles, (2) optical-fibers and (3) textiles-fibers.

Figure 3 presents the FTIR transmission spectra of the TiO_2-deposited luminous textile before and after the photodegradation of CIP. The transmission band observed between 3030 and 2790 cm^{-1} can be attributed to the C-H stretching vibrations of $-CH_3$ and $-CH_2$ groups found in cellulose [28]. In the spectrum of the luminous-textile after the CIP degradation, a decrease in intensity of the C-O peak at 1240 cm^{-1} is evident. This decrease is likely due to the deposition of CIP and its photocatalytic byproducts onto the luminous-textile surface [19]. Additionally, the peak near 1017 cm^{-1} in the spectra of the raw luminous textile, which could be attributed to the carbonyl group of cellulose, shows reduced intensity in the spectra of the luminous textile after CIP degradation.

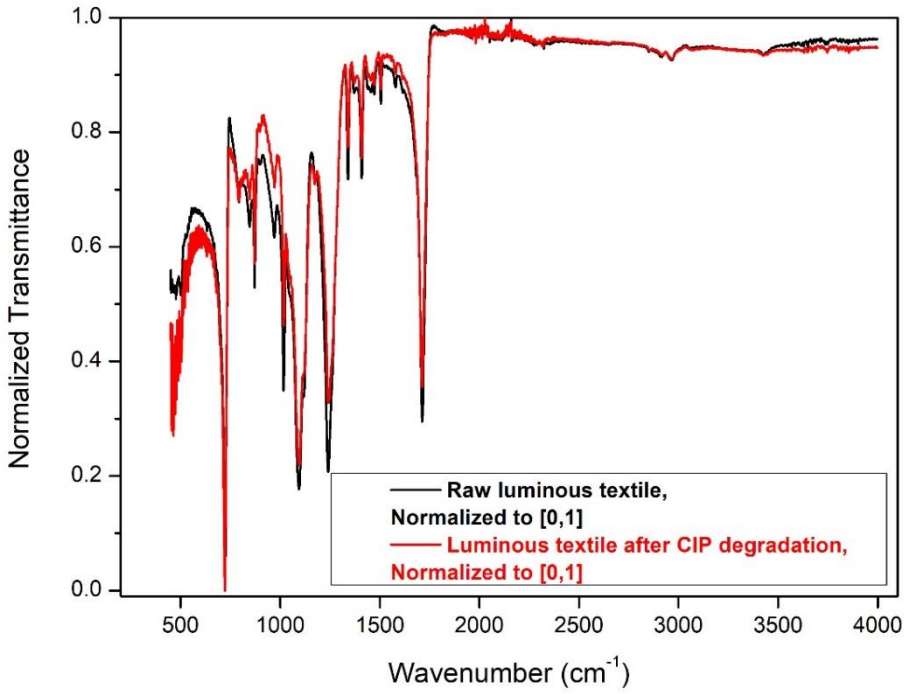

195

196 **Fig. 3** Normalized FTIR spectra of a raw and used (after CIP degradation) luminous
197 textiles.

198 *3.2 Photocatalytic efficiencies of MF, DF, and DF-without TiO_2 luminous textiles*

199 The photocatalytic performances of different luminous textile reactors, namely the
200 "mono-face" (MF), the "double-face" (DF) and the "double-face without TiO_2" (DF-
201 without TiO_2), were compared.

202 The CIP degradation efficiencies of MF, DF and DF-without TiO_2 were monitored
203 over a 360-minute period and presented in **Fig. 4**. On one hand, the luminous textile
204 without TiO_2 support exhibited less than 10% CIP removal efficiency. Thus, it can be
205 concluded that the optical fibers serving as support showed no significant
206 photocatalytic effect. The 10% CIP removal observed could be attributed to
207 adsorptive removal. Moreover, the limited degradation and mineralization efficiency
208 may result from the absence of TiO_2 on the luminous textile surface. It should also be

noted that the CIP could undergo degradation through photolysis under UV light [29]. On the other hand, MF demonstrated approximately 96% removal efficiency. Furthermore, DF exhibited a similar removal trend, achieving nearly100% removal efficiency (**Fig. 4 a**).

The improved removal of CIP by the DF reactor can be attributed to the higher catalytic sites exposed to UV-light and the distribution of optical-fibers on both sides of the DF luminous-textile reactor. In contrast, in the case of the MF reactor, the TiO_2 deposited on the non-luminous faces was not well exposed to UV light. It can be suggested that the catalytic area exposed to UV light is directly proportional to the production of electron-hole pairs. The highest mineralization efficiency, reaching 42%, was achieved using the DF reactor, followed by 37% using the MF reactor (**Fig. 4 b**). It is worth noting that although there is no significant difference in CIP removal between the DF and MF reactors, the mineralization efficiency is enhanced in the DF reactor. This enhanced activity could be attributed to the greater number of active sites available in the DF reactor. In contrast, the DF-without TiO_2 reactor exhibited only 10% CIP removal, and less than 5% mineralization was achieved. This aligns with the hypothesis that without TiO_2, CIP has likely been removed through adsorption and/or photolysis and stored on the fiber surface without being mineralized to CO_2. As demonstrated in **Fig. 3**, the DF reactor exhibited superior performance compared to the other reactors. Therefore, all subsequent experiments were performed using the DF reactor.

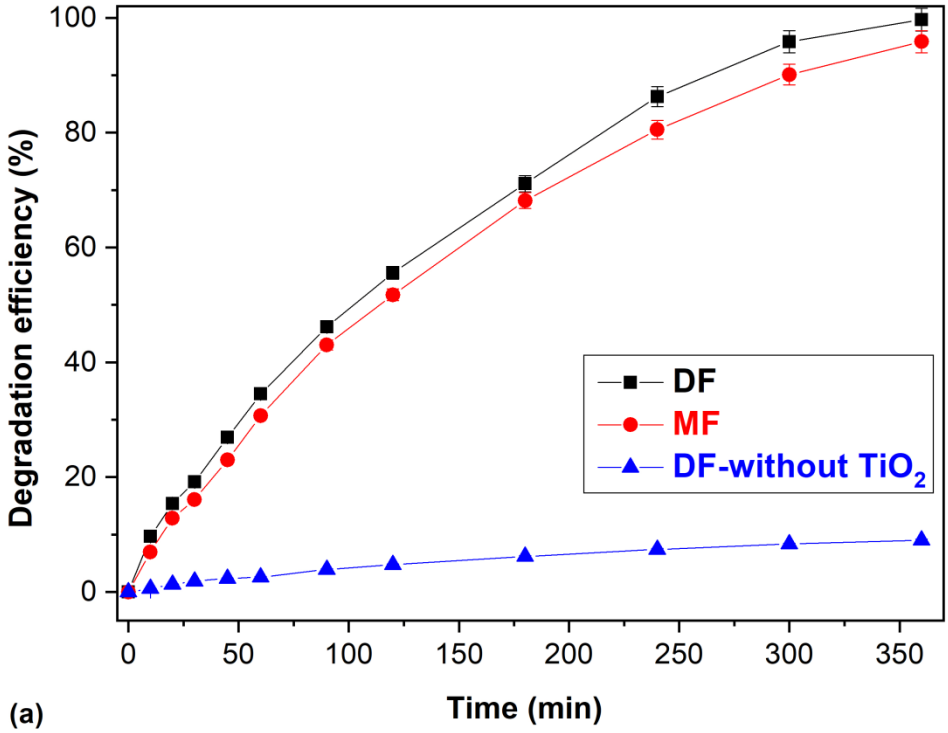
Degradation efficiency (%)
Time (min)
DF
MF
DF-without TiO2

(a)

230

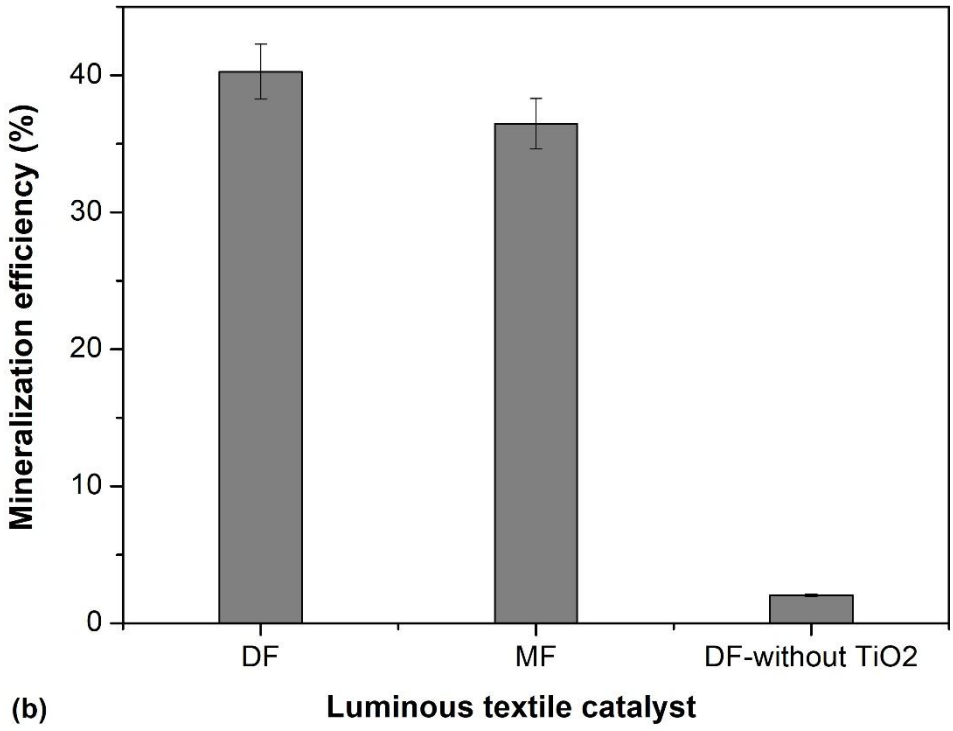
Mineralization efficiency (%)
DF
MF
DF-without TiO2
Luminous textile catalyst

(b)

231

Fig. 4 - Photocatalytic CIP removal efficiencies of MF, DF and DF-without TiO_2 support. **(a)** Degradation, and **(b)** Mineralization efficiency. Initial CIP concentration = 2 mg/L; treatment time = 360 min; UV light intensity = 0.150 mW/cm^2.

3.3 Effect of the CIP initial concentration on degradation efficiency

The influence of the initial CIP concentration on the photocatalytic degradation efficiency, for DF luminous-textile reactor, was investigated for five CIP concentrations in the range of 2 to 10 mg/L. As reported in **Fig. 5 (a),** the degradation efficiency decreased from 99.7% to 28.4% and the mineralization yield decreased from 44.7% to 14.7% after 360 min, when CIP concentration was increased from 2 to 10 mg/L, respectively.

The photocatalytic activity diminishes as the antibiotic concentration rises due to the increased quantity of adsorbed contaminants on the photocatalyst surface. The adsorbed CIP molecules can limit the number of photons reaching the TiO_2 surface. Consequently, the production of reactive oxygen species on the surface also decreases[30]. Additionally, the increase in the initial CIP concentration leads to a reduction in available active sites. Therefore, in a photocatalytic process consisting of successive reactions, the competition for active sites on the catalyst becomes more pronounced.

As depicted in **Fig. 5 (b),** the mineralization efficiency decreased from 40% to 15% as the CIP inlet concentration increased from 2 to 10 mg/L. This observation underscores the importance of the number of available active sites on the TiO_2 surface and the quantity of UV photons reaching the catalyst surface in controlling mineralization. It can be inferred that the optimization of active sites on the surface, which includes factors such as the weight of TiO_2 and the total exposed area, should

256 be based on the pollutant concentration to achieve complete degradation and
257 mineralization.

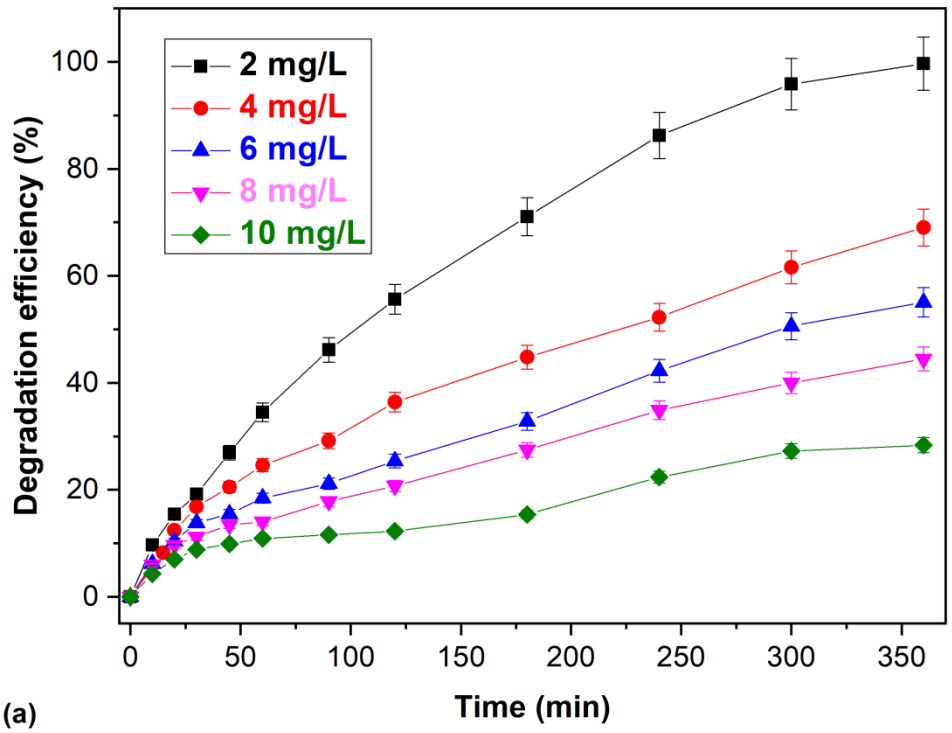

(a)

258

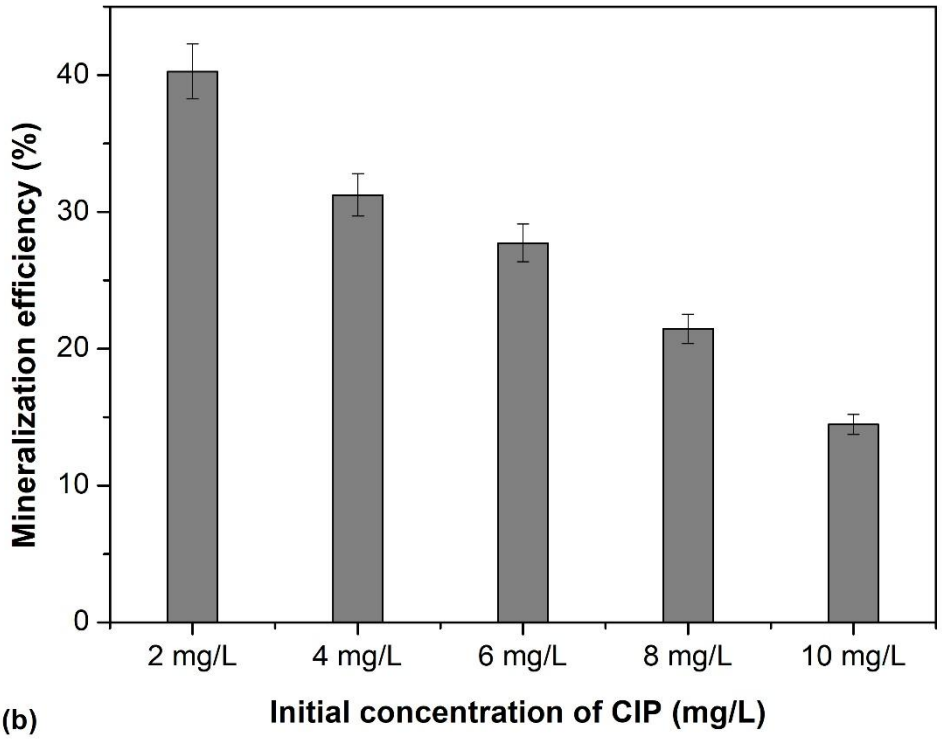

Fig. 5 - Effect of the CIP initial concentration on **(a)** the degradation efficiency and **(b)** the mineralization yield. Reaction time = 360 min; Light intensity = 0.150 mW/cm^2.

The Langmuir–Hinshelwood (L-H) model is employed to comprehend the kinetics of the CIP degradation reaction (Eq.3).

$$\frac{1}{r_0} = \frac{1}{k} + \frac{1}{kK} * \frac{1}{C_0} \qquad \text{Eq. 3}$$

Where k denotes the reaction rate constant (mg L^{-1} min^{-1}), K is the adsorption coefficient of reactants (L mg^{-1}), C_0 is the initial CIP concentration (mg/L) and r_0 is the initial rate of disappearance of CIP (mg L^{-1} min^{-1}). **Fig. 6** displays the linear fitting of $1/r_0$ as a function of $1/C_0$. The linear transformation of this expression yielded values of k = 0.093 mg L^{-1} min^{-1} and K = 0.141 L mg^{-1}. The higher values of R^2 (0.9876) for antibiotic removal indicate that the obtained data fit well with the pseudo first-order kinetic model.

In a study by Zeghioud et al. [31], using the L-H model, the removal of reactive green-12 dye in the presence of TiO_2 impregnated polyester was investigated, and they found k = 0.035 mg L^{-1} min^{-1} and K = 0.796 L mg^{-1}. The kinetic constant obtained in our study is larger than the values reported by Zeghioud et al [31]. This difference may be attributed to the rapid photocatalytic degradation pathways and kinetics of the reactants in the novel reactor design.

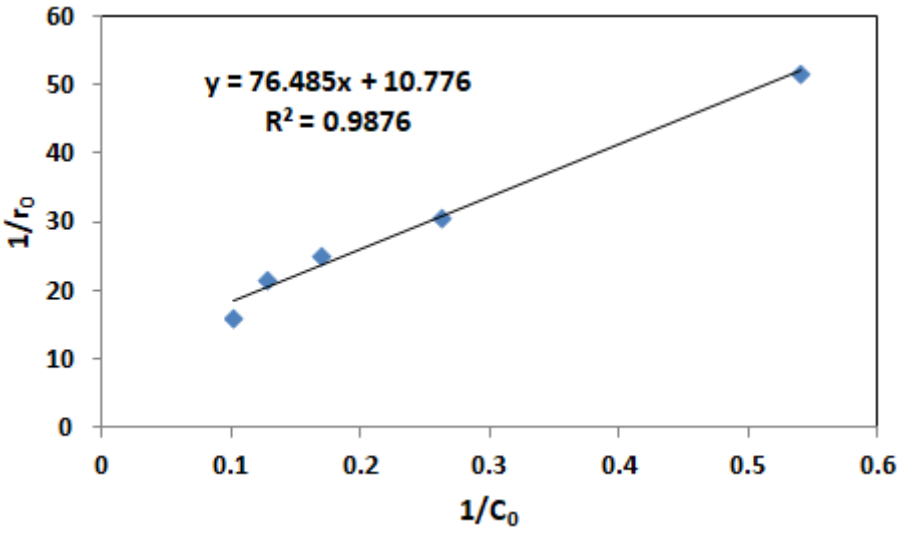

Fig. 6. Linear correlation of $1/r_0$ versus $1/C_0$.

3.4 Effect of UV light intensity on CIP removal

Given that the production of electron-hole pair by UV-light, the UV light intensity is a crucial parameter in antibiotic degradation. To assess the impact of light intensity on the CIP photodegradation process, various experiments were conducted at different light intensities using the DF configuration. The calculated intensities were 0.083, 0.150 and 0.255 mW/cm^2 using three different LED sources. **Figure 7** illustrates the effect of UV light intensity on CIP degradation and mineralization efficiencies.

The results demonstrated that the CIP removal improved as the irradiation intensity increased, which can be attributed to the higher production of hydroxyl radicals on

the catalyst surface. Indeed, under high UV-light intensity, electron-hole pair formation predominates, and the recombination of electron-hole pairs becomes negligible. In contrast, at low UV light intensity, a competition between the separation and recombination of electron-hole pairs occurs, reducing the formation of free radicals and subsequently decreasing antibiotic photodegradation efficiency [19]. The results obtained indicate that the DF luminous textile exhibited highly satisfactory photodegradation rates, even at the lowest light intensity tested. As depicted in **Fig. 7 (b)**, the increase in UV light intensity from 0.083 to 0.255 (3 fold) mW/cm^2 has raised the mineralization efficiency from 27 to 42% (1.6 fold). Overall, it is evident that an increase in UV light intensity has led to an improvement in mineralization. . However, the impact on mineralization is relatively minor. For instance, the ratio between conversion and mineralization for 0.15 and 0.255 mW/cm2 does not exhibit significant changes; specifically, the conversion/mineralization ratio is 2.5 for 0.15 mW/cm^2 and 2.4 for 0.255 mW/cm^2. This finding suggests that the excess UV light intensity has had an insignificant effect on mineralization. Therefore, it can be proposed that CIP mineralization is primarily governed by the interaction between CIP, TiO_2, and UV photons, rather than being solely dependent on the quantity of available photons.

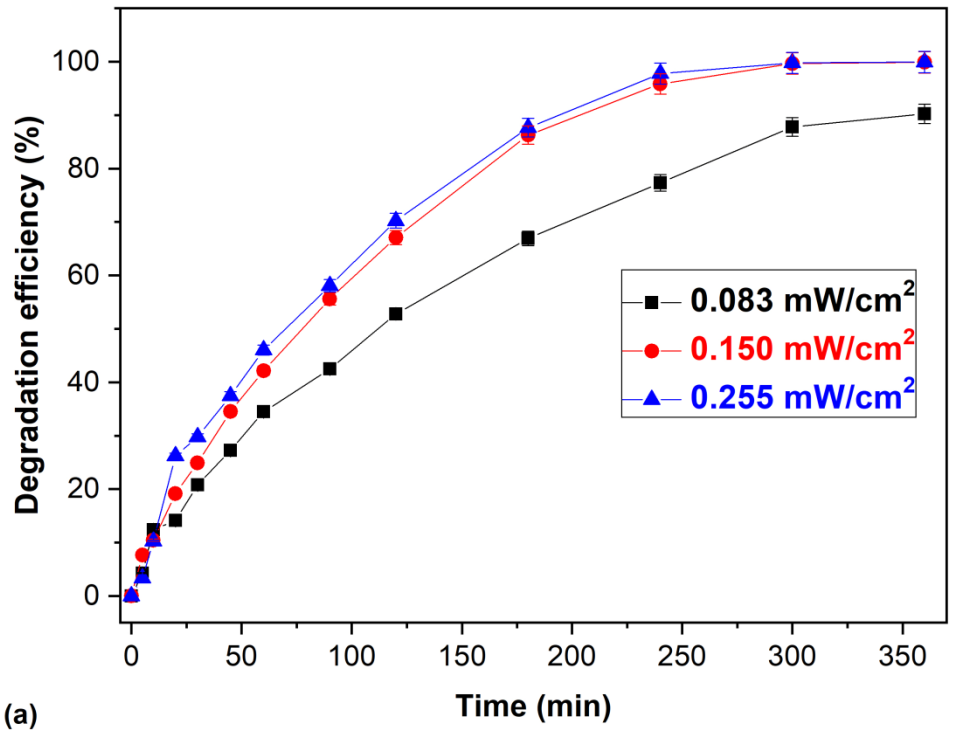
Degradation efficiency (%)
Time (min)
0.083 mW/cm2
0.150 mW/cm2
0.255 mW/cm2

(a)

307

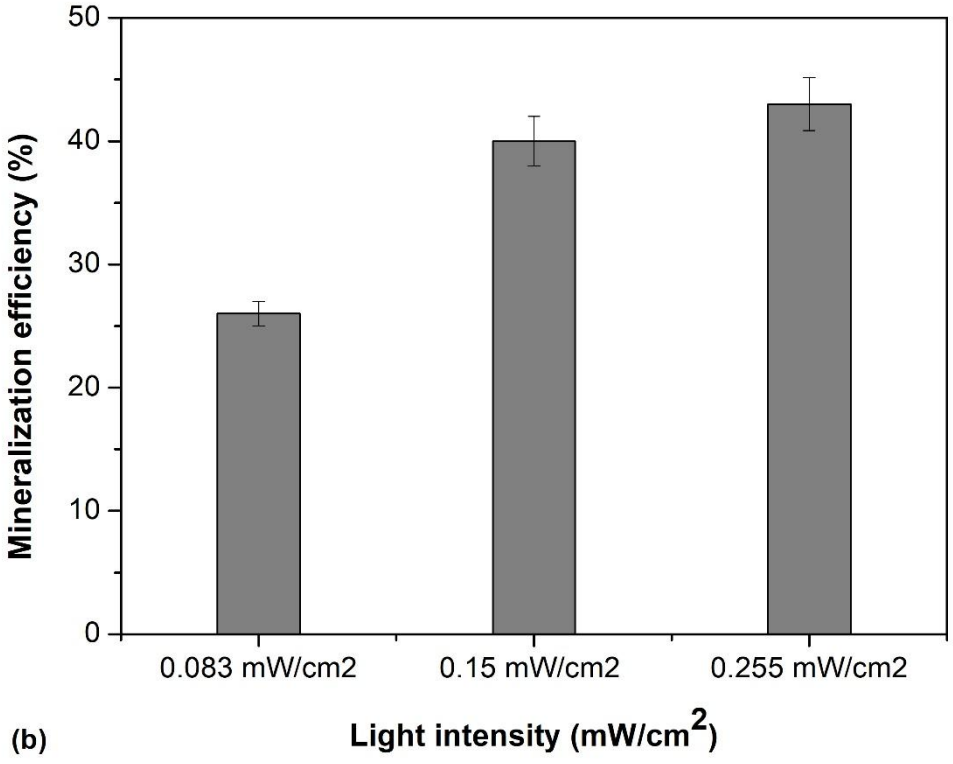
Mineralization efficiency (%)
0.083 mW/cm2
0.15 mW/cm2
0.255 mW/cm2
Light intensity (mW/cm2)

(b)

308

Fig. 7 - Effects of UV intensity on **(a)** the degradation efficiency and **(b)** the mineralization yield. The DF luminous textile reactor, the initial CIP concentration is 2 mg/L, and the reaction time is 360 min.

It has been reported that the activity of the DF luminous-textile is dependent on light irradiation [32]. The relationship between UV light intensity and the rate of pollutant oxidation can be expressed as follows:

$$k_{op} = k_0.I^{\delta} \quad \text{Eq.4}$$

$$\text{Ln } k_{op} = \delta \text{ Ln (I)} + \text{Ln } (k_0) \quad \text{Eq.5}$$

Where K_{op} is the CIP degradation rate (mg L^{-1} min^{-1}), I is the light intensity ($W.m^{-2}$), and k_0 is the rate constant independent of the light intensity and δ is the order of I ($0 < \delta < 1$). When $\delta = 1$, it signifies that the participation of electron-hole pairs in oxidation reactions is faster than their recombination, leading to a linear increase in the CIP oxidation rate with UV light intensity. . When $\delta < 1$, it indicates that the dominant process is the recombination of electron-hole pairs [32]. The k_0 and δ values are provided in **Table 1**, with the δ value confirming that the dominant process in this case is indeed the recombination of electron-hole pairs.

Figure 8 presents **the** kinetic constant for CIP degradation as a function of UV light intensity. It is evident that the CIP degradation rate increased linearly with UV light intensity, indicating that electron-hole pairs were utilized more rapidly for chemical reactions than for recombination[33].

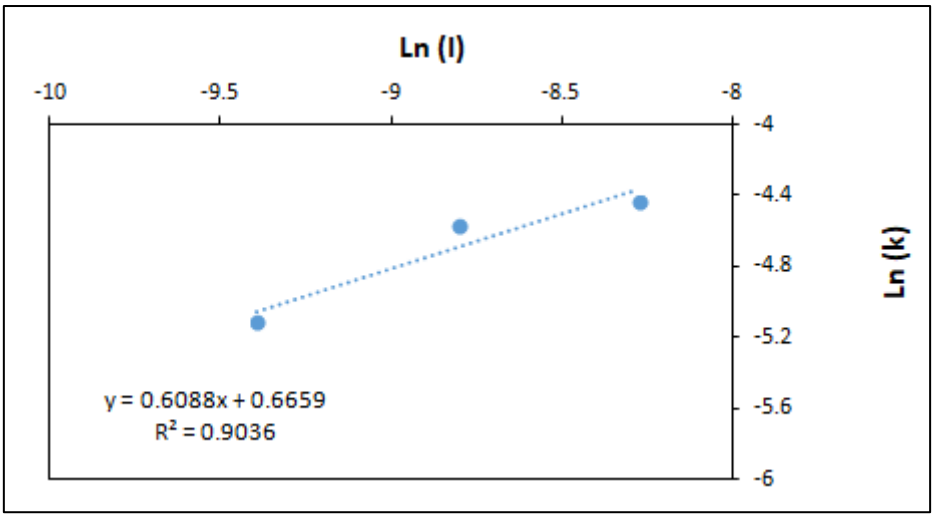

Fig. 8 - Effect of UV light intensity on degradation rate constant for CIP.

Table. 1 Values of the constants δ and k_0.

k_0 (mg L^{-1} min^{-1})	δ	Correlation (%)
0.007	0.61	90.36

3.5 Impact of oxidant addition

3.5.1 Impact of hydrogen peroxide

Various studies have explored the addition of hydrogen peroxide (H_2O_2) to photocatalytic reactors to enhance the production of $^{\bullet}OH$ radicals and facilitate the degradation of refractory organic compounds in water. The production of $^{\bullet}OH$ plays a crucial role in the chemical oxidation of organic pollutants. Additionally, H_2O_2 and its end products are environmentally friendly [34] [35].

The addition of hydrogen peroxide (H_2O_2 serves as an electron acceptor to generate $^{\bullet}OH$ radicals and may reduce the electron-hole recombination (Eq. 6) [36], thereby

potentially improving photocatalytic degradation efficiency. Thus, the influence of H_2O_2 concentrations added to the solution, ranging from 0 to 300 mg/L, was investigated.

$$\bar{e} + H_2O_2 \rightarrow OH^- + {}^{\bullet}OH \quad \text{Eq. 6}$$

Fig. 9 illustrates the impact of the H_2O_2 addition on both k_{app} constant and mineralization yield after 360 min of photocatalytic degradation. It is evident that the k_{app} constant increased as the H_2O_2 concentration was raised from 0 to 150 mg/L. This increase can be attributed to the greater number of ${}^{\bullet}OH$ radicals generated by photocatalytic process. However, beyond a concentration of 150 mg/L of H_2O_2, the k_{app} constant decreased significantly, indicating that an excess of H_2O_2 acts as a scavenger of ${}^{\bullet}OH$ radicals. Additionally, the excess addition of H_2O_2 molecules in the system accelerates the rate of ${}^{\bullet}OH$ radical recombination (Eq. 7):

$$ {}^{\bullet}OH + {}^{\bullet}OH \rightarrow H_2O_2 \quad \text{Eq. 7}$$

As depicted in **Fig. 9**, it is interesting to note that the addition of H_2O_2 did not have a significant impact on mineralization. Almansba et al. [18] and Diez et al., [37] have suggested that some of the generated radicals may react with the produced by-products, potentially reducing the number of available radicals for CIP mineralization. The highest mineralization efficiency of 54.7% was attained with the addition of 150 mg/L of H_2O_2.

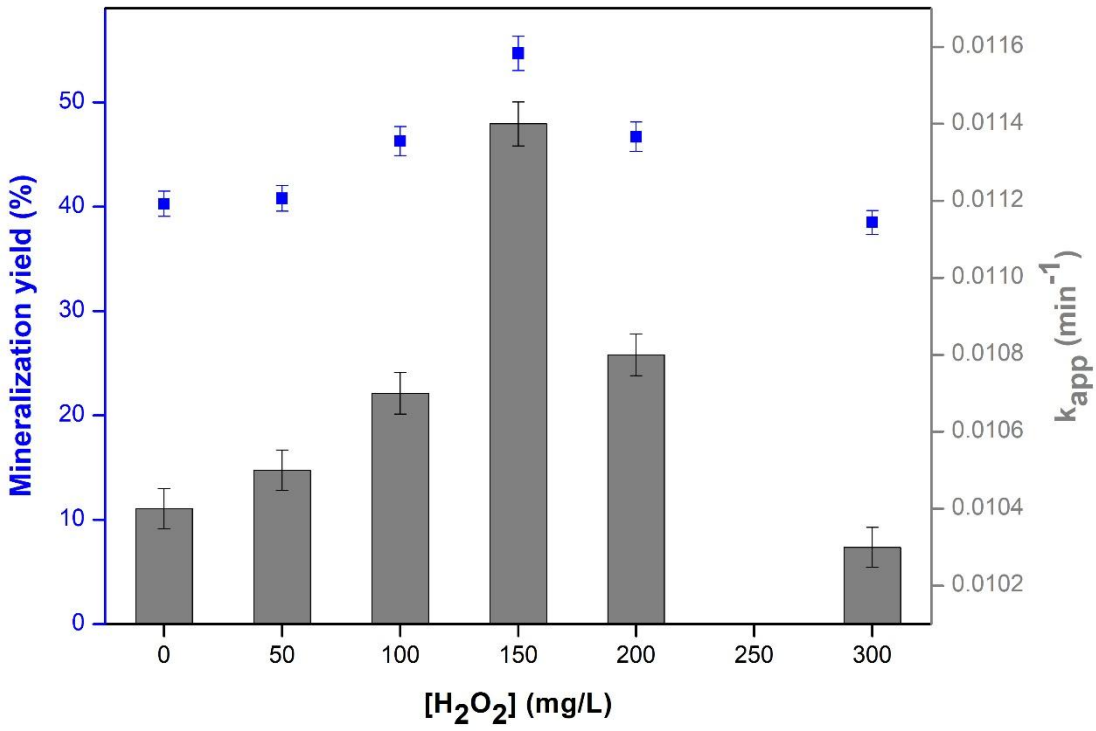

Fig. 9 - Effect of the H_2O_2 concentration on CIP removal kinetic rate constant and the mineralization yield using DF luminous textile reactor. Initial CIP concentration = 2 mg/L; Reaction time = 360 min, Light intensity = 0.15 mW/cm^2

3.5.2 Impact of Persulfate

Persulfate (PS) has been widely utilized to enhance the performance of advanced oxidation process. In the presence of a catalyst, persulfate undergoes cleavage of its O=O bond, leading to the production of sulfate radicals $SO_4^{-\bullet}$, which exhibit a longer half-life and greater selectivity than $^{\bullet}OH$ radicals in water treatment. Several activation methods for PS have been reported, including the use of transition metals, ultrasound and UV irradiation, ultrasound, and carbonaceous materials [34].

Fig. 10 illustrates the impact of the addition of persulfate as an oxidant on both the kinetic rate constant and mineralization efficiency after 360 min of UV irradiation. The

PS addition to the solution enhanced the degradation kinetics. Interestingly, the k_{app} constant increased with increasing PS concentration up to 202 mg/L and then decreased at higher PS concentrations. The initial increase in kapp with higher PS concentration can be attributed to the chemical activation of PS and the generation of sulfate radicals. . However, beyond 202 mg/L of PS, degradation efficiency decreased, which may be explained by the scavenging effect of excess PS on reactive species , as shown in Eq. 8 [38,39].

$$SO_4^{-\bullet} + SO_4^{-\bullet} \rightarrow S_2O_8^{-} \qquad \text{Eq. 8}$$

Furthermore, it is possible that a portion of the generated radicals may react with the by-products formed in the reaction medium. Consequently, the availability of reactive species for CIP mineralization could be significantly reduced. The highest mineralization efficiency, reaching 61.2%, was obtained with the addition 202 mg/L of PS.

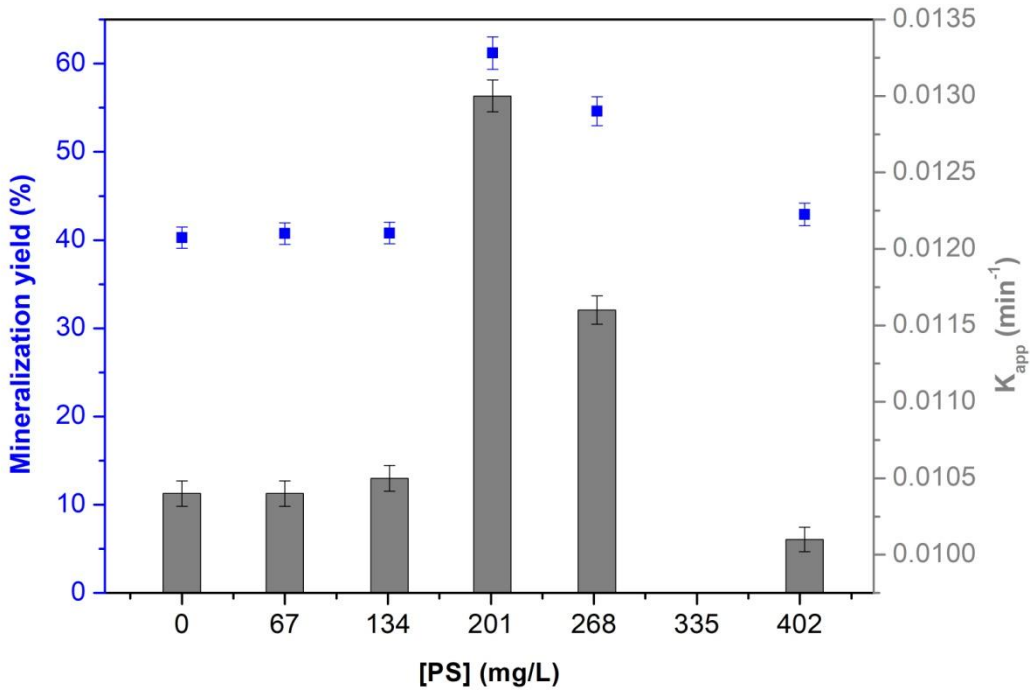

Fig. 10 - Effect of the PS concentration on the kinetic rate constant and the mineralization yield, by the DF luminous textile reactor. Initial CIP concentration = 2 mg/L; Reaction time = 360 min, Light intensity = 0.150 mW/cm^2.

3.6 Effect of radical scavengers on CIP photodegradation

Four scavengers, namely Isopropanol (IPA, 100 mmol/L), tert-Butanol (t-BuOH, 100 mmol/L), Benzoquinone (BQ, 20 µmol/L), and the binary IPA/BQ (Ispr, 100 mmol/L/BQ, 20 µmol/L), were employed to investigate the role of radicals in CIP degradation. Preliminary studies were conducted to determine the optimal concentrations of these scavengers. The respective rate constants and degradation efficiencies were calculated after 360 min of UV irradiation. It is well established that IPA and t-BuOH are used to quench the $^{\bullet}OH$ radicals [40]. Additionally, BQ is considered an effective trap to prevent the formation of the radical couple $HO_2^{\bullet}$ / $O_2^{-\bullet}$ [41]. As depicted in **Fig. 11**, a substantial inhibition was observed following the addition of IPA (k_{app} = 0.0031 min^{-1}), t-BuOH (k_{app} = 0.0041 min^{-1}) and BQ (k_{app} = 0.0050 min^{-1}), providing strong evidence that $HO_2^{\bullet}$, $O_2^{-\bullet}$, and especially $^{\bullet}OH$ radicals, are the primary active species involved in CIP degradation. However, a significant decrease in CIP degradation was observed when the binary mixture of IPA/BQ was added (k_{app} = 0.0013 min^{-1}), suggesting that the $^{\bullet}OH$, $HO_2^{\bullet}$, and $O_2^{-\bullet}$ radicals collectively play the major role in the photocatalytic removal of CIP [40,41].

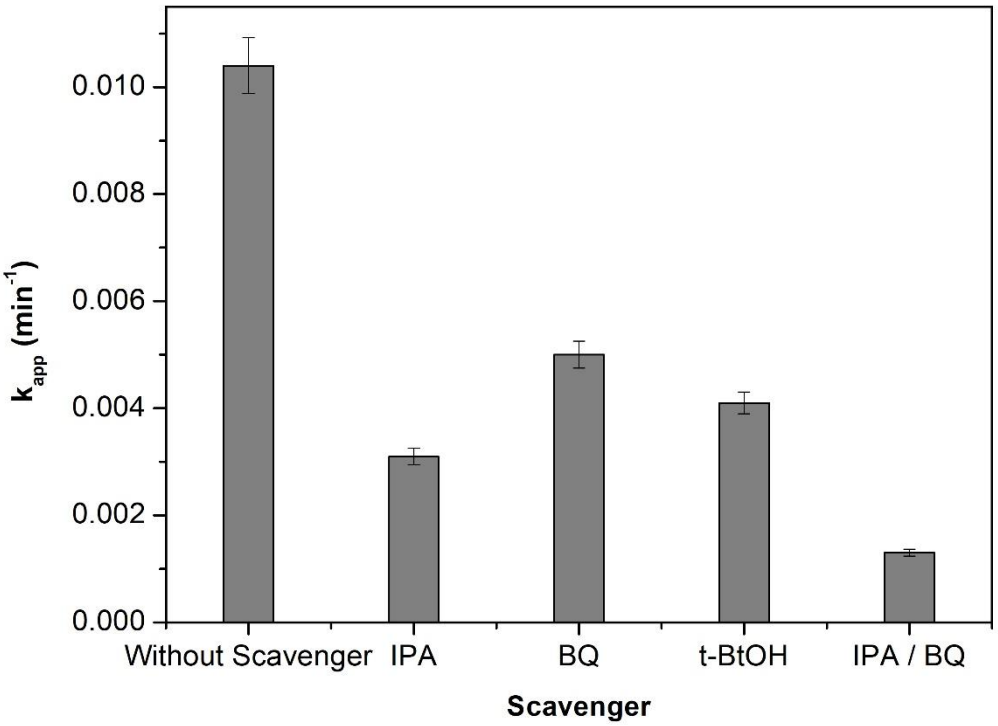

Fig. 11. Effect of the scavengers on the CIP removal kinetics using DF luminous textile reactor. Initial CIP concentration = 2 mg/L; Reaction time = 360 min, Light intensity = 0.15 mW/cm^2, [t-BuOH] = 100 mmol/L, [IPA] = 120 mmol/L, [BQ] = 20 µmol/L.

Heterogenous photocatalysis involves the activation of a solid material like TiO_2 with appropriate high-energy light (hυ), which has energy greater than the material's band gap (Eg =3.2 eV). This high-energy light excites an electron from the valence band (VB) to the conduction band (CB). When an electron moves from the VB to the CB creates an electron/hole (e^-/h^+) pair. The reaction between h^+ holes and electron donors results in the formation of $^{\bullet}OH$ radicals, as depicted in the proposed mechanism through the following equations

$$TiO_2 + h\upsilon \rightarrow e^- + h^+ \qquad \text{Eq. 9}$$

$h^+ + H_2O \rightarrow {}^{\bullet}OH + H^+$ Eq. 10

$h^+ + OH^- \rightarrow {}^{\bullet}OH$ Eq. 11

It was also reported that the interaction between the excited electron e^- and the dioxygen can give rise to the formation of oxygen superoxide radicals, as shown below

$O_2 + e^- \rightarrow O_2^{-\bullet}$ Eq. 12

$O_2^{-\bullet} + H^+ \rightarrow HO_2^{\bullet}$ Eq. 13

The proposed mechanism of CIP photocatalysis is depicted in **Fig. 12.**

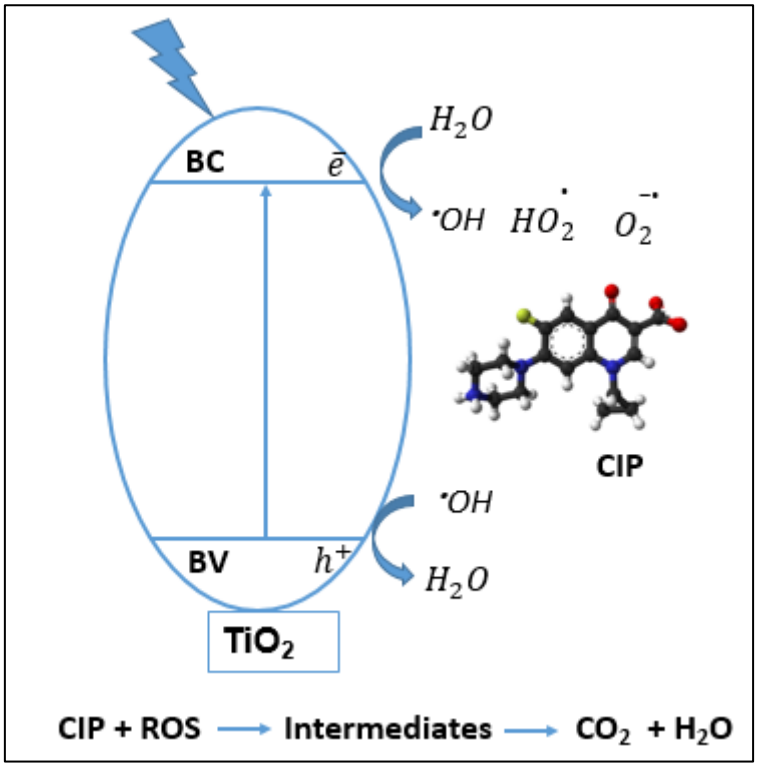

Fig. 12 – proposed mechanism of CIP photocatalysis

3.7 Effects of water matrices on CIP removal and mineralization efficiencies

The impact of different water matrices, including nitrate (NO_3^-), chloride (Cl^-), sulfate (SO_4^{2-}), and carbonates ($CO_3^{2-}$and HCO_3^-) on CIP degradation efficiency and mineralization has been investigated under similar operating conditions using the DF reactor. The experiments were conducted with different water sources: ultrapure water (UPW), tap water (TW), and synthetic water (SW), and the results are presented in Fig. **13.** The fundamental physicochemical properties of these various water matrices, as previously described in our study [27], are outlined in **Table 2.** It is worth noting that TW and SW contain nitrate, chloride, sulfate, and nitrite ions, which are absent in the UPW solution.

Table. 2 Physic-chemical properties of various water matrices.

Parameters	UPW	TW	SW
pH	5.8	7.8	7.6
Conductivity (µS/ cm)	15.12	492.2	2454
Nitrates (NO_3^-, mg/ L)	-	8.6 ± 0.4	8.2 ± 0.4
Nitrites (NO_2^-, mg/ L)	-	< 0.02	< 0.02
Sulfate (SO_4^{2-}, mg/ L)	-	6.6 ± 0.3	6.4 ± 0.3
Chloride (Cl^-, mg/ L)	-	36.3 ± 1.8	234 ± 6

The results show that CIP degradation was notably faster in UPW compared to TW and SW. The reduced CIP degradation and mineralization efficiencies in TW and SW compared to UPW can be attributed to the composition of the water matrix, specifically the presence of various ions in the solution. Previous research has demonstrated the detrimental impact of nitrate, chloride, sulfate, and bicarbonate ions on photocatalysis [18,19,27,42].The inhibitory effect of nitrate anions may be due to

their relatively large size, which could potentially block active sites on the catalyst surface [43]. Nitrate anions might reduce the availability of holes and radicals by scavenging them, as indicated in the following equations [42]:

$$NO_3^- + h^+ \leftrightarrow NO_3^{\bullet} \quad \text{Eq. 14}$$

$$NO_3^- + {}^{\bullet}OH \leftrightarrow NO_3^{\bullet} + OH^- \quad \text{Eq. 15}$$

Additionally, the mechanisms of electron-hole scavenging by chloride and sulfate ions were elucidated in the study conducted by Almansba et al. [18], as outlined below :

$$SO_4^{2-} + h^+ \leftrightarrow SO_4^{-\bullet} \quad \text{Eq. 16}$$

$$SO_4^{2-} + {}^{\bullet}OH \leftrightarrow SO_4^{-\bullet} + OH^- \quad \text{Eq. 17}$$

$$Cl^- + h^+ \leftrightarrow Cl^{\bullet} \quad \text{Eq. 18}$$

$$Cl^- + {}^{\bullet}OH \leftrightarrow Cl^{\bullet} + OH^- \quad \text{Eq. 19}$$

Furthermore, the decline in photocatalytic activity can be associated with the presence of bicarbonate ions in TW, which have the potential to trap ${}^{\bullet}OH$ radicals, as demonstrated in the following equations [19]:

$$HCO_3^- + {}^{\bullet}OH \leftrightarrow CO_3^{-\bullet} + H_2O \quad \text{Eq. 20}$$

$$CO_3^{2-} + {}^{\bullet}OH \leftrightarrow CO_3^- + OH^- \quad \text{Eq. 21}$$

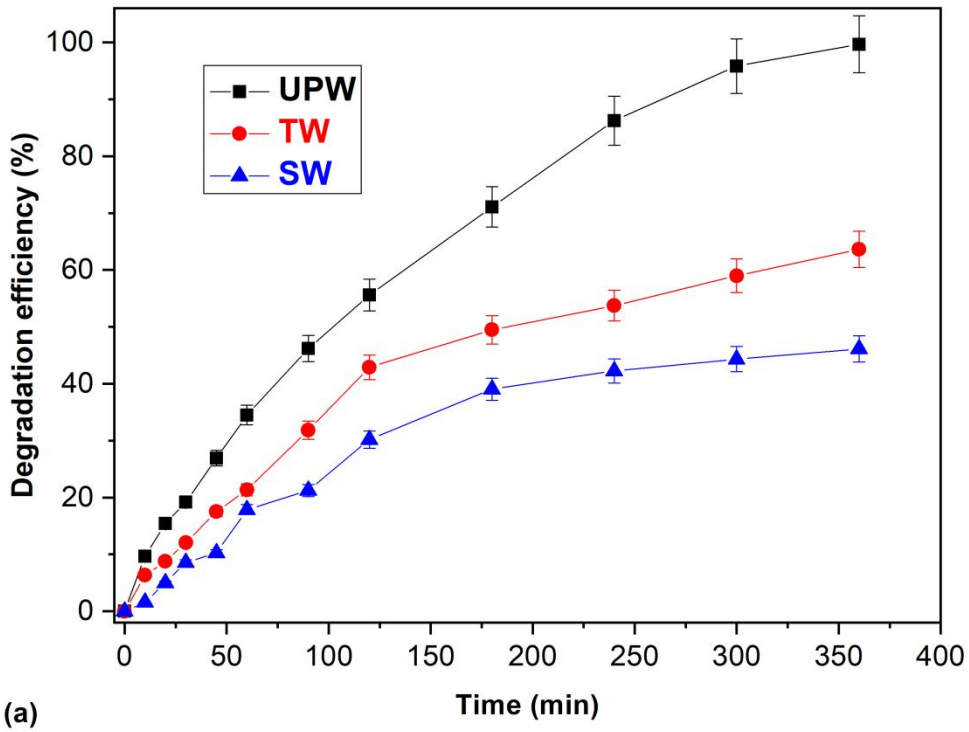
UPW
TW
SW
Degradation efficiency (%)
Time (min)
0
20
40
60
80
100
0
50
100
150
200
250
300
350
400

(a)

463

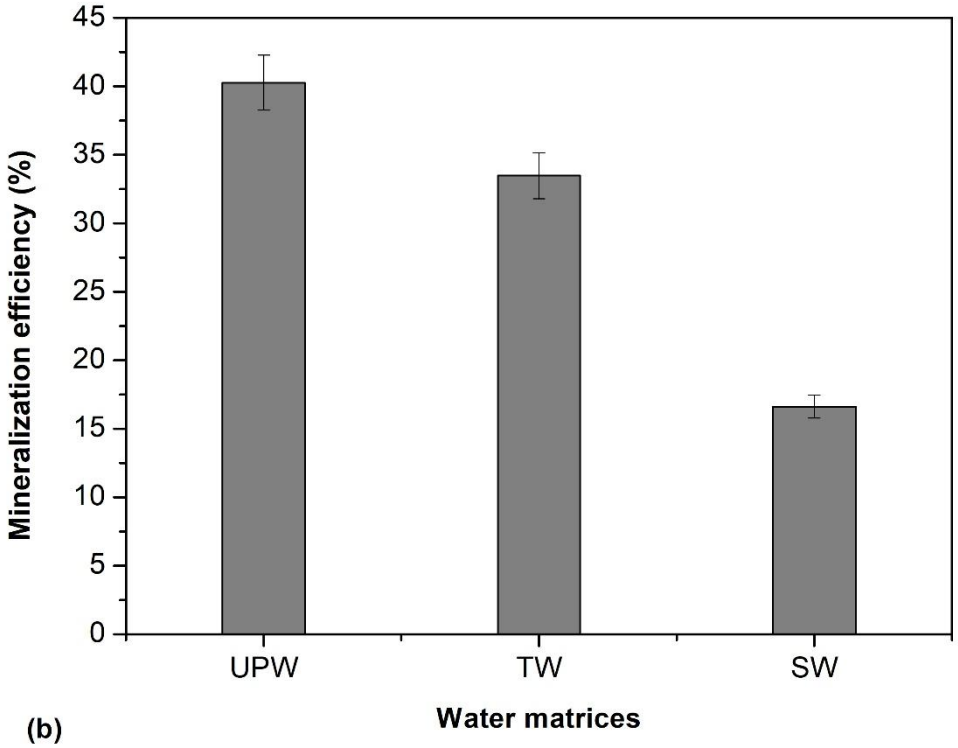
Mineralization efficiency (%)
Water matrices
UPW
TW
SW
0
5
10
15
20
25
30
35
40
45

(b)

464

Fig. 13 - Effect of water matrices on the CIP removal by the DF configuration. **(a) CIP** degradation efficiency and **(b)** mineralization yield. Initial CIP concentration = 2 mg/L; Reaction time = 360 min, Light intensity = 0.150 mW/cm^2. Abbreviations: UPW = ultra-pure water, TW = tap water, SW = synthetic water.

Table .2 Literature comparison of pollutants removal from water by luminous textile catalysts

Target pollutant	Operating Conditions	%RE	%TOC	References
Paracetamol	$[pollutant]_0$ = 1 mg/L Reaction time = 340 min	95.7	-	[44]
Flumequine	$[pollutant]_0$ = 20 mg/L Reaction time = 330 min Water matrices : UPW	76	38	[18]
Flumequine	$[pollutant]_0$ = 20 mg/L Reaction time = 330 min Water matrices : TW	61	26	[18]
Formic acid	$[pollutant]_0$ = 2 mg/L Reaction time = 30 min	23-60	-	[14]
phenol	$[pollutant]_0$ = 2 mg/L Reaction time = 30 min	6-8	-	[14]
Flumequine	$[pollutant]_0$ = 2.5 mg/L Reaction time = 330 min	87	40	[45]
CIP	$[pollutant]_0$ = 2 mg/L Reaction time = 360 min Water matrices : UPW	99.7	40.3	This work
CIP	$[pollutant]_0$ = 2 mg/L Reaction time = 360 min Water matrices : TW	63.6	33.5	This work
CIP	$[pollutant]_0$ = 2 mg/L Reaction time = 360 min Water matrices : SW	46.1	16.7	This work

Table 2 provides a summary of the results obtained in previous studies regarding the photocatalytic degradation of various pollutants using luminous textile catalysts. These results are compared to the findings from the current study. It is evident that

the photocatalytic performance of the utilized catalyst in this study exceeded the results reported for other luminous textiles. This suggests that the material used in this study is an effective catalyst for the degradation of CIP. Additionally, while most of the reported studies were conducted in UPW, the experiments in this work encompassed UPW, TW, and SW, providing a more comprehensive understanding of the catalyst's performance under various water matrices.

4. Conclusion

In this study, the degradation of CIP in a compact batch reactor using a photocatalytic luminous textile reactor was thoroughly examined. The "double-face" (DF) luminous textile reactor exhibited the highest degradation efficiency (99.7%) and mineralization yield (40.3%) compared to the "mono-face" (MF) and "double-face without TiO_2" (DF-without TiO_2) luminous textiles. This improved performance can be attributed to the uniform distribution of TiO_2 on the optical fibers' surfaces on both sides of the DF reactor, enhancing CIP removal and by-product mineralization. Characterization of the optical fibers of the DF reactor before and after photocatalytic reactions using FTIR and SEM confirmed the uniform TiO_2 distribution, further supporting its role in enhancing CIP degradation and mineralization. The study revealed that the efficiency of CIP degradation and mineralization decreased as the initial concentration of CIP increased or as the UV light intensity decreased. The most favorable photocatalytic activity was observed when the initial CIP concentration was at 2 mg/L, and the UV light intensity was 0.15 mW/cm^2. The decrease in photocatalytic activity at higher CIP concentrations can be attributed to the limited availability of active sites on the catalyst surface. When the concentration of CIP is high, these active sites can become saturated with CIP molecules, reducing the number of available sites for photocatalytic reactions. Under conditions of low UV

light intensity, there is a competition between the separation and recombination of electron-hole pairs. This competition results in fewer free radicals being formed, leading to a decrease in the efficiency of CIP photodegradation. In essence, at lower UV light intensities, the rate of electron-hole recombination becomes more pronounced, impeding the formation of the reactive radicals necessary for effective photocatalysis.

The highest k_{app} constant (0.0114 min^{-1}) and mineralization level (54.7%) were achieved with 150 mg/L of H_2O_2. The addition of H_2O_2 generated $^{\bullet}OH$ radicals, reduced the electron-hole recombination, and enhanced the photocatalytic efficiency. Furthermore, the introduction of H_2O_2 molecules into the system increased the rate of $^{\bullet}OH$ radical recombination. Additionally, the highest k_{app} constant (0.0130 min^{-1}) and mineralization level (61.2%) were attained with 202 mg/L of PS. The inclusion of PS as an oxidant to the solution resulted in faster degradation kinetics. However, an excess of PS molecules in the system led to the scavenging effect of reactive species. The addition of oxidants significantly improved the photocatalytic performance of the luminous textile. The study explored the influence of various scavengers on CIP degradation, confirming that $HO_2^{\bullet}$, $O_2^{-\bullet}$, and $^{\bullet}OH$ radicals, played pivotal roles in the CIP degradation reaction. Furthermore, the photocatalytic performance of luminous textile was assessed in different water matrices, shedding light on the underlying mechanisms of CIP degradation involving various oxidative processes. The results revealed that CIP degraded more rapidly in ultra-pure water (UPW) compared to tap water (TW) and synthetic water (SW). The degradation efficiency decreased progressively from 99.7% in UPW to 63.6% in TW and 46.1% in SW. This decrease in efficiency could be attributed to the detrimental effects of nitrate, chloride, sulfate, and carbonate ions present in TW and SW, which negatively

impacted TiO2 photocatalysis, resulting in reduced CIP degradation efficiency and mineralization yields. In summary, this study showcased the remarkable photocatalytic prowess of the luminous textile for degrading the antibiotic CIP. This was achieved by enhancing the interaction between CIP, the catalyst surface, and UV light. Additionally, the use of LED technology significantly reduced energy consumption, making this approach highly promising for environmental applications.

References

[1] M. Thakur, D. Pathania, Environmental fate of organic pollutants and effect on human health, Elsevier Inc., 2019. doi:10.1016/B978-0-12-818095-2.00012-6.

[2] M. Bilal, M. Adeel, T. Rasheed, Y. Zhao, H.M.N. Iqbal, Emerging contaminants of high concern and their enzyme-assisted biodegradation – A review, Environment International. 124 (2019) 336–353. doi:10.1016/j.envint.2019.01.011.

[3] C. Agabo-garcía, G. Repetto, M. Albqmi, G. Hodaifa, Evaluation of the olive mill wastewater treatment based on advanced oxidation processes (AOPs), flocculation , and filtration, Journal of Environmental Chemical Engineering. 11 (2023) 109789. doi:10.1016/j.jece.2023.109789.

[4] S. Karoui, R. Ben Arfi, K. Mougin, A. Ghorbal, A.A. Assadi, A. Amrane, Synthesis of novel biocomposite powder for simultaneous removal of hazardous ciprofloxacin and methylene blue: Central composite design, kinetic and isotherm studies using Brouers-Sotolongo family models, Journal of Hazardous Materials. 387 (2020) 121675. doi:10.1016/j.jhazmat.2019.121675.

[5] A.L. Ahmad, S.W. Puasa, Reactive dyes decolourization from an aqueous

549 solution by combined coagulation/micellar-enhanced ultrafiltration process,
550 Chemical Engineering Journal. 132 (2007) 257–265.
551 doi:10.1016/j.cej.2007.01.005.

552 [6] S. Karoui, R. Ben Arfi, K. Mougin, A. Ghorbal, A.A. Assadi, A. Amrane,
553 Synthesis of novel biocomposite powder for simultaneous removal of
554 hazardous ciprofloxacin and methylene blue : Central composite design ,
555 kinetic and isotherm studies using Brouer-Sotolongo family models, Journal of
556 Hazardous Materials. 387 (2019) 121675. doi:10.1016/j.jhazmat.2019.121675.

557 [7] M. De Kwaadsteniet, P.H. Dobrowsky, A. Van Deventer, W. Khan, T.E. Cloete,
558 Domestic rainwater harvesting: Microbial and chemical water quality and point-
559 of-use treatment systems, Water, Air, and Soil Pollution. 224:1629 (2013).
560 doi:10.1007/s11270-013-1629-7.

561 [8] A. Yusuf, H. Kehinde, J. Olanrewaju, A. Giwa, O. Pikuda, A. Dindi, M. Roil,
562 Hazardous and emerging contaminants removal from water by plasma-based
563 treatment : A review of recent advances, Chemical Engineering Journal
564 Advances. 14 (2023) 100443. doi:10.1016/j.ceja.2023.100443.

565 [9] S. yong Lu, D. Wu, Q. lin Wang, J. Yan, A.G. Buekens, K. fa Cen,
566 Photocatalytic decomposition on nano-TiO2: Destruction of chloroaromatic
567 compounds, Chemosphere. 82 (2011) 1215–1224.
568 doi:10.1016/j.chemosphere.2010.12.034.

569 [10] A. V. Karim, A. Hassani, P. Eghbali, P. V. Nidheesh, Nanostructured modified
570 layered double hydroxides (LDHs)-based catalysts: A review on synthesis,
571 characterization, and applications in water remediation by advanced oxidation
572 processes, Current Opinion in Solid State and Materials Science. 26 (2022).

573 doi:10.1016/j.cossms.2021.100965.

574 [11] A. Hassani, P. Eghbali, F. Mahdipour, S. Wacławek, K.Y.A. Lin, F. Ghanbari,
575 Insights into the synergistic role of photocatalytic activation of
576 peroxymonosulfate by UVA-LED irradiation over CoFe2O4-rGO
577 nanocomposite towards effective Bisphenol A degradation: Performance,
578 mineralization, and activation mechanism, Chemical Engineering Journal. 453
579 (2023). doi:10.1016/j.cej.2022.139556.

580 [12] O. Baaloudj, I. Assadi, N. Nasrallah, A. El Jery, L. Khezami, A.A. Assadi,
581 Simultaneous removal of antibiotics and inactivation of antibiotic-resistant
582 bacteria by photocatalysis: A review, Journal of Water Process Engineering. 42
583 (2021) 102089. doi:10.1016/j.jwpe.2021.102089.

584 [13] A. Molino, M. Hamandi, R. Grosjean, F. Dappozze, L. Lamaa, L. Peruchon, C.
585 Brochier, K. Demb, M. El Hajem, P. Vernoux, C. Guillard, H. Kaper, Coupling of
586 photocatalysis and catalysis using an optical fiber textile for room temperature
587 depollution, Chemosphere. 297 (2022) 133940.
588 doi:10.1016/j.chemosphere.2022.133940.

589 [14] C. Indermühle, E. Puzenat, F. Dappozze, F. Simonet, L. Lamaa, L. Peruchon,
590 C. Brochier, C. Guillard, Photocatalytic activity of titania deposited on luminous
591 textiles for water treatment, Journal of Photochemistry and Photobiology A:
592 Chemistry. 361 (2018) 67–75. doi:10.1016/j.jphotochem.2018.04.047.

593 [15] M. Hamandi, N. Ha- Son, D. Frédéric, L. Lina, P. Laure, B. Cédric, C. Guillard,
594 Application of Luminous Textile Coated by Tio2 For Photocatalytic Removal of
595 Acetic Acid, Formaldehyde and Toluene from Indoor Air, Journal of Textile
596 Science & Fashion Technology. 2 (2019). doi:10.33552/jtsft.2019.02.000546.

[16] W. Abou Saoud, A. Kane, P. Le Cann, A. Gerard, L. Lamaa, L. Peruchon, C. Brochier, A. Bouzaza, D. Wolbert, A.A. Assadi, Innovative photocatalytic reactor for the degradation of VOCs and microorganism under simulated indoor air conditions: Cu-Ag/TiO2-based optical fibers at a pilot scale, Chemical Engineering Journal. 411 (2021) 128622. doi:10.1016/j.cej.2021.128622.

[17] M. Abidi, A.A. Assadi, A. Bouzaza, A. Hajjaji, B. Bessais, S. Rtimi, Photocatalytic indoor/outdoor air treatment and bacterial inactivation on CuxO/TiO2 prepared by HiPIMS on polyester cloth under low intensity visible light, Applied Catalysis B: Environmental. 259 (2019). doi:10.1016/j.apcatb.2019.118074.

[18] A. Almansba, A. Kane, N. Nasrallah, R. Maachi, L. Lamaa, L. Peruchon, C. Brochier, B. Imane, M. Unilasalle-ecole, Innovative photocatalytic luminous textiles optimized towards water treatment : Performance evaluation of photoreactors, Chemical Engineering Journal. 416 (2021) 129195. doi:10.1016/j.cej.2021.129195.

[19] S. Karoui, R. Ben Arfi, A. Ghorbal, A. Amrane, A.A. Assadi, Innovative sequential combination of fixed bed adsorption/desorption and photocatalysis cost-effective process to remove antibiotics in solution, Progress in Organic Coatings. 151 (2020) 1–10.

[20] A. Labella, M. Gennari, V. Ghidini, I. Trento, A. Manfrin, J.J. Borrego, M.M. Lleo, High incidence of antibiotic multi-resistant bacteria in coastal areas dedicated to fish farming, Marine Pollution Bulletin. 70 (2013) 197–203. doi:10.1016/j.marpolbul.2013.02.037.

[21] G. Gunawan, N.B.A. Prasetya, R.A. Wijaya, Degradation of Ciprofloxacin (CIP)

621 antibiotic waste using the advanced oxidation process (AOP) method with
622 ferrate (VI) from exterme base electrosynthesis, (2023) 6639.
623 doi:http://doi.org/10.48048/tis.2023.6639.

624 [22] W. Fu, M. Qin, H. Niu, Q. Hu, D. Guo, M. Chen, C. Niu, D. Huang, Insights into
625 the high performance of Co – Mn oxide supported by carbon fiber frameworks
626 for ciprofloxacin oxidation process, Journal of Cleaner Production. 392 (2023)
627 136062. doi:10.1016/j.jclepro.2023.136062.

628 [23] F. Ghanbari, F. Zirrahi, D. Olfati, F. Gohari, A. Hassani, TiO2 nanoparticles
629 removal by electrocoagulation using iron electrodes: Catalytic activity of
630 electrochemical sludge for the degradation of emerging pollutant, Journal of
631 Molecular Liquids. 310 (2020) 113217. doi:10.1016/j.molliq.2020.113217.

632 [24] M.R. Khavari Kashani, R. Kiani, A. Hassani, A. Kadier, S. Madihi-Bidgoli,
633 K.Y.A. Lin, F. Ghanbari, Electro-peroxone application for ciprofloxacin
634 degradation in aqueous solution using sacrificial iron anode: A new hybrid
635 process, Separation and Purification Technology. 292 (2022) 121026.
636 doi:10.1016/j.seppur.2022.121026.

637 [25] C. Indermühle, E. Puzenat, F. Simonet, L. Peruchon, C. Brochier, C. Guillard,
638 Modelling of UV optical ageing of optical fibre fabric coated with TiO_2, Applied
639 Catalysis B: Environmental. 182 (2016) 229–235.
640 doi:10.1016/j.apcatb.2015.09.037.

641 [26] P. Bourgeois, E. Puzenat, L. Peruchon, F. Simonet, D. Chevalier, E. Deflin, C.
642 Brochier, C. Guillard, Characterization of a new photocatalytic textile for
643 formaldehyde removal from indoor air, “Applied Catalysis B, Environmental.”
644 128 (2012) 171–178. doi:10.1016/j.apcatb.2012.03.033.

645 [27] S. Karoui, W. Abou, A. Ghorbal, F. Fourcade, A. Amrane, A. Amin,
646 Intensification of non-thermal plasma for aqueous Ciprofloxacin degradation :
647 Optimization study , mechanisms , and combined plasma with photocatalysis,
648 Journal of Water Process Engineering. 50 (2022) 103207.
649 doi:10.1016/j.jwpe.2022.103207.

650 [28] R. Ben Arfi, S. Karoui, K. Mougin, C. Vaulot, L. Josien, G. Schrodj, L. Michelin,
651 A. Ghorbal, Enhanced Malachite Green uptake using chemically-modified reed-
652 based powder : equilibrium , kinetics , mechanism , and reusability Enhanced
653 Malachite Green uptake using chemically-modified, International Journal of
654 Environmental Analytical Chemistry. (2020) 1–19.
655 doi:10.1080/03067319.2020.1828389.

656 [29] O.S. Keen, K.G. Linden, Degradation of antibiotic activity during UV/H2O2
657 advanced oxidation and photolysis in wastewater effluent, Environmental
658 Science and Technology. 47 (2013) 13020–13030. doi:10.1021/es402472x.

659 [30] A.A. Azzaz, A.A. Assadi, S. Jellali, A. Bouzaza, D. Wolbert, S. Rtimi, L.
660 Bousselmi, Discoloration of simulated textile effluent in continuous photoreactor
661 using immobilized titanium dioxide: Effect of zinc and sodium chloride, Journal
662 of Photochemistry and Photobiology A: Chemistry. 358 (2018) 111–120.
663 doi:https://doi.org/10.1016/j.jphotochem.2018.01.032.

664 [31] H. Zeghioud, N. Khellaf, A. Amrane, H. Djelal, W. Elfalleh, A.A. Assadi, S.
665 Rtimi, Photocatalytic performance of TiO_2 impregnated polyester for the
666 degradation of Reactive Green 12: implications of the surface pretreatment and
667 the microstructure, “Journal of Photochemistry and Photobiology, A:
668 Chemistry.” 346 (2017) 493–501.

669 doi:http://dx.doi.org/doi:10.1016/j.jphotochem.2017.07.005 JPC.

670 [32] A.A. Assadi, J. Palau, A. Bouzaza, D. Wolbert, Modeling of a continuous
671 photocatalytic reactor for isovaleraldehyde oxidation: Effect of different
672 operating parameters and chemical degradation pathway, Chemical
673 Engineering Research and Design. 91 (2013) 1307–1316.
674 doi:10.1016/j.cherd.2013.02.020.

675 [33] J. Palau, J.M. Penya-Roja, C. Gabaldón, F. Javier Álvarez-Hornos, F.
676 Sempere, V. Martínez-Soria, UV photocatalytic oxidation of paint solvent
677 compounds in air using an annular TiO_2-supported reactor, Wiley Online
678 Library. 86 (2011) 273–281. doi:10.1002/jctb.2515.

679 [34] A. Hassani, J. Scaria, F. Ghanbari, P. V Nidheesh, Sulfate radicals-based
680 advanced oxidation processes for the degradation of pharmaceuticals and
681 personal care products : A review on relevant activation mechanisms ,
682 performance , and perspectives, Environmental Research. 217 (2023) 114789.
683 doi:10.1016/j.envres.2022.114789.

684 [35] M. Kumar, S. Ambika, A. Hassani, P. V Nidheesh, Waste to catalyst : Role of
685 agricultural waste in water and wastewater treatment, Science of the Total
686 Environment. 858 (2023) 159762. doi:10.1016/j.scitotenv.2022.159762.

687 [36] Z. Liu, Z. Liu, X. Sheng, D. Wang, X. Feng, Efficient Hydrogen Peroxide
688 Generation Utilizing Photocatalytic Oxygen Reduction at a Triphase Interface,
689 ISCIENCE. 17 (2019) 67–73. doi:10.1016/j.isci.2019.06.023.

690 [37] A.M. Díez, F.C. Moreira, B.A. Marinho, J.C.A. Espíndola, L.O. Paulistab, M.A.
691 Sanromána, M. Pazosa, R.A.R. Boaventurab, V.J.P. Vilar, A step forward in

692 heterogeneous photocatalysis : Process intensi fi cation by using a static mixer
693 as catalyst support, Chemical Engineering Journal. 343 (2018) 597–606.
694 doi:10.1016/j.cej.2018.03.041.

695 [38] C. Tan, D. Fu, N. Gao, Q. Qin, Y. Xu, H. Xiang, Kinetic degradation of
696 chloramphenicol in water by UV / persulfate system, “Journal of
697 Photochemistry & Photobiology, A: Chemistry.” 332 (2017) 406–412.
698 doi:10.1016/j.jphotochem.2016.09.021.

699 [39] M.S.P. Yadav, N. Neghi, M. Kumar, G.K. Varghese, Photocatalytic-oxidation
700 and photo-persulfate-oxidation of sulfadiazine in a laboratory-scale reactor :
701 Analysis of catalyst support , oxidant dosage , removal-rate and degradation
702 pathway, Journal of Environmental Management. 222 (2018) 164–173.
703 doi:10.1016/j.jenvman.2018.05.052.

704 [40] G.N. Coulibaly, S. Rtimi, A.A. Assadi, K. Hanna, Nano-sized iron oxides
705 supported on polyester textile to remove fluoroquinolones in hospital
706 wastewater, Environmental Science Nano. 7 (2020) 2156–2165.
707 doi:10.1039/D0EN00261E.

708 [41] M. Kamagate, A. Amin, T. Kone, L. Coulibaly, K. Hanna, Activation of
709 persulfate by irradiated laterite for removal of fluoroquinolones in multi-
710 component systems, Journal of Hazardous Materials. 346 (2018) 159–166.
711 doi:10.1016/j.jhazmat.2017.12.011.

712 [42] B. Chládková, E. Evgenidou, L. Kvítek, A. Panáček, R. Zbořil, P. Kovář, D.
713 Lambropoulou, Adsorption and photocatalysis of nanocrystalline TiO2 particles
714 for Reactive Red 195 removal: effect of humic acids, anions and scavengers,
715 Environmental Science and Pollution Research. 22 (2015) 16514–16524.

716 doi:10.1007/s11356-015-4806-y.

717 [43] A.M. Dugandžić, A. V. Tomašević, M.M. Radišić, N. Šekuljica, D. Mijin, S.D.
718 Petrović, Effect of inorganic ions, photosensitisers and scavengers on the
719 photocatalytic degradation of nicosulfuron, Journal of Photochemistry and
720 Photobiology A: Chemistry. 336 (2017) 146–155.
721 doi:10.1016/j.jphotochem.2016.12.031.

722 [44] H. Dhibi, M. Guiza, A. Bouzaza, A. Ouederni, L. Lamaa, L. Péruchon, C.
723 Brochier, A. Amrane, S. Loganathan, S. Rtimi, A.A. Assadi, Photocatalytic
724 degradation of paracetamol mediating luminous textile: Intensification of the
725 chemical oxidation, Journal of Water Process Engineering. 53 (2023) 103648.
726 doi:10.1016/j.jwpe.2023.103648.

727 [45] A. Almansba, A. Kane, N. Nasrallah, J.M. Wilson, R. Maachi, L. Lamaa, L.
728 Peruchon, C. Brochier, A. Amrane, A.A. Assadi, An engineering approach
729 towards the design of an innovative compact photo-reactor for antibiotic
730 removal in the frame of laboratory and pilot-plant scale, Journal of
731 Photochemistry and Photobiology A: Chemistry. 418 (2021).
732 doi:10.1016/j.jphotochem.2021.113445.

733